University of Reading

School of Mathematical and Physical Sciences

Department of Mathematics and Statistics

Rain drop growth by collision and coalescence

Peter Barnet

August 2011

Abstract

The numerical scheme proposed by Bott to simulate the growth of cloud droplets is used to investigate the aspects to which the collision and coalescence growth mechanism is sensitive. Perturbations to the initial size and concentration of the cloud droplets are considered, as well as modifications to the shape of the initial droplet distribution. The impact of these changes on the time taken for the model to produce drops of rain size is determined. The collision kernel governing the chance of cloud droplets colliding and coalescing is also studied to gauge an understanding of the likelihood of this process happening for certain size drops.

It is demonstrated that the relationship between the time taken to produce rain t and the total water content w, (the droplet concentration) for drops of constant size is $t \propto w^{-1}$. The relationship between the size of the droplets and the time taken to produce rain is shown to vary depending on the droplet size, with three different regimes existing. For large droplets of radius $r > 300\mu m$ the relation $t \propto r^2$ approximately holds, which disagrees with theoretical derivations that point to a cubic relationship. Through analysing the collision kernel it is revealed that the chance of two droplets colliding and coalescing is extremely sensitive to the size of the colliding drops.

Chapter 1

Introduction

A fundamental problem with existing models that simulate the growth of cloud water droplets into raindrops, is that they do not predict the process to happen fast enough in convective clouds. Even though these models are not used to produce weather forecasts, and are purely for research purposes, they are very important for furthering our understanding of the processes to which cloud droplet growth is sensitive. There are two mechanisms by which this droplet growth occurs; diffusion of excess moisture in the cloud onto the cloud droplets, and through collision and coalescence of the cloud droplets. Out of these two growth mechanisms, the latter is the dominant for drops of radius larger than about 10 μm (Davis and Sartor 1967), whereas for drops smaller than this the moisture diffusion mechanism is more important.

The collision and coalescence process refers to two cloud droplets of different sizes (and hence masses) coming into contact because there terminal velocities are different. If when they collide, they then stick together to form

a new drop of mass equal to the sum of the two original droplet masses, then we say the drops have coalesced. The following schematic highlights a situation when collision and coalescence may occur.
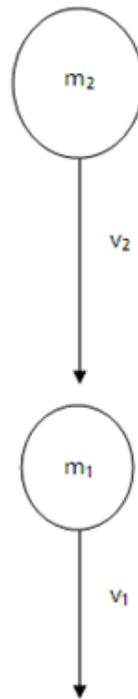

Figure 1.1: schematic of how two drops can collide

In this schematic (figure 1.1) a drop of mass m_2 falling at terminal velocity v_2 is on course to collide with a smaller drop of mass m_1 falling at its terminal velocity v_1, since $v_2 > v_1$. If the two drops combine (coalesce) when they collide then we obtain the situation shown in figure 1.2.
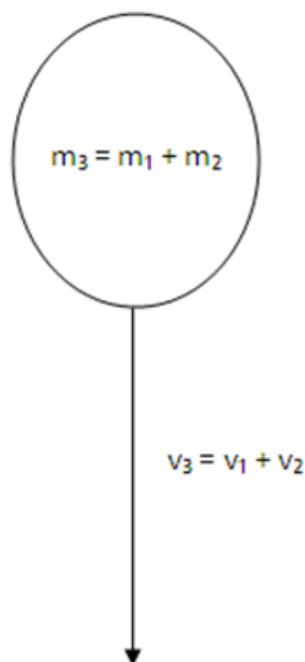
$$m_3 = m_1 + m_2$$

$$v_3 = v_1 + v_2$$

Figure 1.2: schematic of coalesced drops

The new drop that forms has mass that is simply the sum of the two colliding droplet masses, and terminal velocity equal to the sum of the velocities of the colliding drops. The larger of the two colliding drops is referred to as the collector drop and is considered to be drop that gains the mass at the expense of the smaller drop in the collision. This smaller drop is usually called the collected drop.

The collision and coalescence of cloud droplets is quite a complicated process, and one reason for this is the fact that an initial droplet size spectrum must

be known in great detail. More importantly though, we need to correctly calculate the chance of droplets colliding and coalescing, because this is known to be sensitive to the droplet radii. Previous work on this particular aspect of the problem by Hocking (1959) had shown that collision was impossible unless the collector drop had a radius larger than 18 μm. The reason why the collector drops must be greater than a certain size for the collision and coalescence process to occur, is the fact that small cloud droplets have almost insignificant mass and hence little inertia. This lack of inertia results in droplets changing their trajectories to avoid collisions (if they are sufficiently small), through following the flow of the air around each other. Davis and Sartor (1967) were able to improve the estimate of the minimum size of the collector drops, and showed that they can in fact be as small as 10 μm, though at this size the collection efficiency (described next) is low.

Even if two droplets collide, they do not necessarily coalesce, and it is this principle that leads to the so called collection efficiency. This term can be thought of as the product of the collision efficiency and the coalescence efficiency. The collision efficiency represents the probability of two given drops colliding, and the coalescence efficiency refers to the chance of two collided drops combining to form one single drop. Beard and Ochs (1984) were able to show that the coalescence efficiency decreases with increasing drop sizes, from near 100 percent for collector drop radii R < 25 μm and collected droplet radii r < 10 μm, to 50 percent or less for R > 800 μm and r > 40 μm. This therefore suggests that the low collection efficiency obtained by Davis and Sartor for R = 10 μm is due to the very low collision efficiency for

collector drops this small (associated with the drops following the air flow around eachother and avoiding collision).

When two droplets collide it can result in the break up of the collector drop, or simply the two drops moving apart fairly unchanged. Davis and Sartor (1967) illustrated that overall the collection efficiency is dominated by the collision efficiency, with the coalescence efficiency playing a less significant role. For this reason the collection efficiency largely follows the variation of the collision efficiency with droplet radius, and so it is lower for collisions between small drops than it is for collisions between larger drops.

Analytically the collision and coalescence growth mechanism is treated as a stochastic (random) process due to the fact that whether two drops collide and coalesce or not is based on chance. The equation governing the process is called the stochastic collection equation (SCE) and is as follows (Pruppacher and Klett 1997).

$$\frac{\partial n(x,t)}{\partial t} = \int_{x_0}^{x_1} n(x_c,t)K(x_c,x')n(x',t)dx' - \int_{x_0}^{\infty} n(x,t)K(x,x')n(x',t)dx'$$

(1.1)

In equation 1.1, $n(x,t)$ is the drop number distribution function at a given time t, and $K(x_c,x')$ is the collection kernel which describes the rate at which drops of mass $x_c = x - x'$ are collected by drops of mass x', to form a new drop of mass x. x_0 corresponds to the smallest drop being involved in the collection process and $x_1 = x/2$. As in Berry (1967), instead of writing the

SCE in terms of the change in the drop number distribution function with time, we can write it in terms of the change in the mass distribution function $g(y,t)$, where

$$g(y,t)dy = xn(x,t)dx, \quad n(x,t) = \frac{1}{3x^2}g(y,t).$$

(1.2)

Here $y = \ln r$ with r being the radius of the drops with mass x. The mass distribution function basically describes how the total water mass is distributed in drops of different sizes. If we substitute (1.2) into (1.1) we obtain the SCE describing the change in the mass distribution function with time,

$$\frac{\partial g(y,t)}{\partial t} = \int_{y_0}^{y_1} \frac{x^2}{x_c^2 x'} g(y_c,t)K(y_c,y')g(y',t)dy' - \int_{y_0}^{\infty} g(y,t)\frac{K(y,y')}{x'}g(y',t)dy'$$

(1.3)

where $y_c = \ln r_c$ and $y' = \ln r'$ with r_c and r' being the radius of drops of mass x_c and x' respectively. The first integral on the right hand side of (1.3) represents the rate at which drops of mass x are gained by collision and coalescence of two smaller drops. The second integral describes the loss of drops of mass x due to collection by other drops.

In this paper we will explore the aspects to which the collision and coalescence growth mechanism is sensitive, with the aim of trying to explain how the rapid formation of rain seen in convective clouds is possible. To do this we use a numerical method devised by Bott (1998), which solves the SCE in the form of equation (1.3) using a finite volume approach. Details of

the scheme Bott used are given in the following section.

1.1   Numerical methods for solving the SCE

A popular numerical method to approximate the SCE was devised by Berry and Reindhart (1974). They solved (1.1) at discrete points of the drop spectrum giving very accurate results. However the problem with the scheme they used was that due to the number of calculations that must be made, the method was not very computationally efficient and so it was slow to yield results.

A new flux (finite volume) method was proposed in 1998 by Bott. The instant advantage of this method over the scheme devised by Berry and Reindhart is that it is very computationally efficient. The method Bott devised is now briefly described, but greater detail can be found in Bott (1998).

To solve (1.3) numerically a logarithmically equidistant mass grid was introduced,

$$x_{k+1} = \alpha x_k, \quad k = 1, ..., m, \tag{1.4}$$

where x_{k+1} corresponds to the mass in grid box $k + 1$ and x_k to the mass in grid box k. From 1.4 we yield the y grid mesh equally spaced with $\Delta y_k = \Delta y = \ln \alpha / 3$. It should be noted that m is the total number of grid points, and $\alpha = 2^{\frac{1}{2}}$, which results in a doubling of the drop mass after two

grid boxes. $\Delta y_k = \ln \alpha/3$ from the fact that $y = \ln r$ and $x \propto r^3$ (which we know from the relation $Mass = Density \times Volume$, where $Volume = \frac{4}{3}\pi r^3$). Since α can be thought of as a change in mass, we can write $y \propto \ln \alpha^{\frac{1}{3}}$. It therefore follows that because we are considering the grid spacing (change in y over a grid box), we can write $\Delta y_k = \ln \alpha^{\frac{1}{3}}$ which is just expressed more simply as $\Delta y_k = \ln \alpha/3$.

The collision of drops with mass x_i with drops of mass x_j yields a change in the mass distributions g_i, g_j. In discretized form the change in the mass distributions may be expressed as,

$$g_i(i,j) = g_i - g_i \frac{K(i,j)}{x_j} g_j \Delta y \Delta t \tag{1.5}$$

$$g_j(j,i) = g_j - g_j \frac{K(j,i)}{x_i} g_i \Delta y \Delta t \tag{1.6}$$

In these discretizations, g_i and g_j represent the mass distribution functions at grid point i and j respectively before the collision, while $g_i(i,j)$ and $g_j(j,i)$ are the new distributions after the collision. $K(i,j)$ is the collection Kernel for collisions between these drops (described later in this section), and Δt is the time step being considered. These discretizations have this form because in both (1.5) and (1.6) we are considering the mass distribution functions to reduce (because less drops exist with mass x_i and x_j after the collision) and so we are considering the second integral (the rate of mass loss) in equation (1.3). So (1.5) and (1.6) are just discretizations of the second integral in (1.3).

Collisions between drops in grid box i with drops in grid box j produce new drops of mass $x'(i,j) = x_i + x_j$, and so we obtain the mass distribution function $g'(i,j)$ for the new drops formed, which is can be discretized as:

$$g'(i,j) = \frac{x'(i,j)}{x_i x_j} g_i K(i,j) g_j \Delta y \Delta t \tag{1.7}$$

Discretization (1.7) has this form because $g'(i,j)$ has increased as a result of the collisions leading to drops of mass $x'(i,j)$. This means that we are therefore considering the first integral in (1.3), representing the rate of mass gain, and hence (1.7) is just a discretization of the first integral.

A problem exists that $x'(i,j)$ usually differs from the discretized mass points x_k, meaning

$$x_k \leq x'(i,j) \leq x_{k+1}, \tag{1.8}$$

and so the mass density $g'(i,j)$ must be split up in the grid boxed k and $k+1$. Bott (1998) did this partitioning by the following two-step procedure. Firstly the entirety of $g'(i,j)$ is added to grid box k so that,

$$g'_k(i,j) = g_k + g'(i,j). \tag{1.9}$$

Secondly a certain fraction of $g'_k(i,j)$ is transported into grid box $k+1$. The calculations made treat this mass transport as an advection process through the boundary $k + \frac{1}{2}$ between the grid boxes k and $k+1$. The procedure is

9
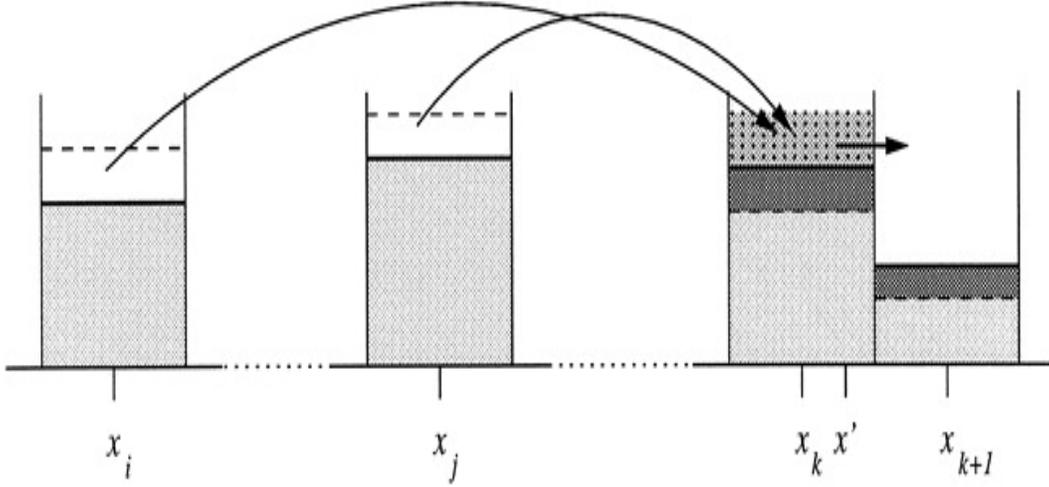
shown in the following schematic by Bott.

Figure 1.3: Schematic illustration of the flux method (Bott 1988)

In figure 1.3, the dashed lines represent the initial mass distributions in grid boxes i, j, k, and $k+1$, and the full lines indicate the mass distributions after the collision process. The stippled area in grid box k corresponds to the mass that will be transported into grid box $k + 1$, and the dark shaded areas are the final mass increase in grid boxes k and $k + 1$.

This mass advection may be written as,

$$g_k(i, j) = g'_k(i, j) - f_{k+1/2}(i, j) \qquad (1.10)$$

$$g_{k+1}(i, j) = g_{k+1} + f_{k+1/2}(i, j), \qquad (1.11)$$

where

$$\frac{f_{k+1/2}(i,j)\Delta y}{\Delta t}$$

represents the mass flux through the boundary $k + \frac{1}{2}$. To obtain the results in this paper we will calculate $f_{k+1/2}(i,j)$ using the upstream formula Bott proposed, although it should be noted he tried two additional approaches to determine the flux. The upstream formula gives,

$$f_{k+1/2}(i,j) = c_k g'_k(i,j) w(i,j). \tag{1.12}$$

In this formula we should interpret c_k as a Courant number, and should calculate it as a function of the position $x'(i,j)$ between x_k and x_{k+1} as below.

$$c_k = \frac{x'(i,j) - x_k}{x_{k+1} - x_k} \tag{1.13}$$

A weighting function $w(i,j)$ has been introduced in (1.12) because the advective flux through the boundary $k + \frac{1}{2}$ is given by $g'(i,j)$ instead of $g'_k(i,j)$, unlike for the normal advection process with $c_k = 1$ (for $x'(i,j) = x_{k+1}$). As a result,

$$w(i,j) = \frac{g'(i,j)}{g'_k(i,j)}, \tag{1.14}$$

and hence it is clear that the upstream scheme is simply,

$$f_{k+1/2}(i,j) = c_k g'(i,j). \tag{1.15}$$

This results in the same partitioning of $g'(i,j)$ as that in the method of Kovetz and Olund (1969), except they solved the SCE in terms of number distribution, as in (1.1). Bott found that this upstream formula produces drop spectra that are seemingly too broad, and he knew this to be due to the large numerical diffusion that results from such an advection scheme. The two other approaches he tried determined the flux according to higher order advection schemes of Bott (1989a,b), and through using these the numerical diffusion was reduced.

An iterative procedure is needed in order to treat all the collisions of drops during the time step Δt. If the grid box of the smallest and largest drops being involved in the collision process are denoted by $i = i_0$ and $i = i_1$, then firstly collision of the smallest drops with drops of grid box $j = i_0 + 1$ is calculated giving new mass distribution functions according to equations (1.5),(1.6),(1.10) and (1.11). Next the collision of the drops remaining in $i = i_0$ having the new mass distribution function $g_{i_0}(i_0, i_0 + 1)$ with the drops in grid box $j = i_0 + 2$ is determined. This process is continued until all the collisions of drops in grid box $i = i_0$ with drops of grid boxes $j = i_0 + 1, i_0 + 2, ..., i_1$ have been considered. Next collisions of drops in grid box $i = i_0 + 1$ with all larger drops $j = i_0 + 2, i_0 + 3, ..., i_1$ are treated in the same way, and this is repeated for all drops $i = i_0 + 2, ...$, until in the last

12

step the collision of drops $i = i_1 - 1$ with drops $j = i_1$ has been determined.

It is clear from equations (1.5) and (1.6) that $g_i(i, j)$ or $g_j(j, i)$ could become negative which is obviously a problem because negative mass concentrations are unphysical. It is therefore required that the flux method is positive definite, and this can be insured by applying the following restrictions to the numerical time step:

$$\Delta t \leq \frac{x_j}{g_j(i, j - 1)\Delta y K(i, j)} \tag{1.16}$$

$$\Delta t \leq \frac{x_i}{g_i(i, j - 1)\Delta y K(i, j)} \tag{1.17}$$

where inequality (1.17) is valid for $j \neq k$. The first inequality (1.16) ensures that $g_i(i, j) \geq 0$ after each collision. The reason why (1.17) does not apply if $j = k$ is that for $j = k$ the mass subtracted from $g_j(j, i)$ in (1.6) will be added again in (1.9).

Earlier in this section the collection kernel $K(i, j)$ was mentioned, and this quantity is related to the probability that in a given time interval there will be a collection event involving two droplets. In Bott's model three different calculation methods are considered for the kernel, these including the Golovin kernel (taken from Golovin 1963), and the hydrodynamic kernels. The Golovin kernel will not be described or used at any point to obtain results in this paper, however results are presented for the other two kernels,

and so these are now briefly described.

The hydrodynamic kernel is given (from Pruppacher and Klett 1997) by the following:

$$k(i, j) = \pi(r_i + r_j)^2 E \, |w(r_i) - w(r_j)| \qquad (1.18)$$

In (1.18) r_i and r_j represent the radii of the two colliding drops respectively, and $w(r_i)$, $w(r_j)$ correspond to the terminal velocities of the two drops, obtained following Beard (1976). E is the collision efficiency and in this report we will consider two different methods for determining its value, one of which is taken from Long (1974), and is calculated as:

$$E = k_1 r_1^2 \left(\frac{1 - k_2}{r_2} \right). \qquad (1.19)$$

In (1.19) r_1 refers to the radius of the collector drop, and r_2 to the drop being collected and k_1, k_2 are constants of value $4.5 \times 10^4 cm^{-2}$ and $3 \times 10^{-4} cm$ respectively. Here we see the large dependence on the colliding droplet radii, as all 3 contributions to (1.18) consider drop size. It is this kernel with the collection efficiency calculated as (1.19) that we will use to produce most of the results that are described in this paper.

The second approach that Bott used to obtain values of E in (1.18) involved using a data table of colliding drop radii and collision efficiencies from Hall (1980). The table consists of results derived by various authors, as for

14

collector drops of radius $< 30\mu m$ Hall chose the theoretical results of Davis (1972) and Jonas (1972). For collecting droplets of radii between 40 and 300 μm, which are collecting smaller drops with radius $< 60\%$ the size of the collector drop radius the results of Schlamp *et al.* (1976), Lin and Lee (1975) and Shafrir and Gal-Chen (1971) were chosen. If the radii ratio was greater than 0.6 (for the same radius range) Hall chose to use the results of Klett and Davis (1973).

Chapter 2

Methodology

From the previous work on this field it appears that the growth process is sensitive to both the size and the initial concentration of droplets within the cloud. In order to quantify the growth rate of these model simulated drops, we introduce a function that calculates the time taken to produce rain drops in the cloud. Since raindrops can be a large range of sizes, a fixed radius value had to be chosen in the model, so as to be consistent for comparisons. This radius was chosen to be 1mm, which is a typical radius for a raindrop in a convective cloud. The model from Bott (1998) was adapted so as to indicate that rain was being produced when more than 50 percent of the total water in the cloud was in drops of radius greater than 1mm, this way avoiding the issue that chance collisions might produce a few drops of this size very quickly, which would lead to the model suggesting a growth rate that may be unrealistically fast.

As stated earlier, in Bott's simulations the initial mode radius of the cloud

drops was chosen to be 10 μm, with the size distribution in the form of a single peak, for which the total water content was fixed at 1 gm^{-3}. An ideal first set of perturbations to try would therefore be to investigate the effect of changing both the initial mode radius and the total water content. In doing this we are effectively changing both the initial size and concentration of the cloud drops, since if we just increase the radius, and keep the total water fixed at 1 gm^{-3}, the droplet field we obtain will have larger but fewer drops compared to the field considered by Bott. If we were however to increase the initial radii and total water by the same factor, we would obtain larger drops than Bott considered, but the concentration of drops would be the same. Through investigating the effect of making these perturbations, it should be possible to determine a relationship between these parameters and the time taken to produce drops that are sufficiently large to be rain. It should be noted that for these perturbations we will be using the hydrodynamic collision kernel with the collision efficiency calculated according to Long.

The effect of having two peaks in the initial droplet size distribution will also be investigated, as this will allow us to clearly observe how the two different sizes of droplets interact and form larger drops. A series of additional perturbations will be made to the model for an initial two peak distribution, including changing the method for calculating the collision efficiency to that of Hall. This will allow us to examine whether the droplet evolution differs substantially or not for the two different collision efficiencies. To examine the kernels further we will determine the magnitudes of the three components that make them up, from which we should be able to see how the contribu-

tion from the collision efficiency differs for the different calculation methods (as the contribution from $(r_i + r_j)^2$ and $w(r_i) - w(r_j)$ will be the same in each case). This breaking up of the kernel will also allow us to observe the relative importance of the three componence under different collision scenarios (different sizes of droplets colliding).

Chapter 3

Results

We first examine the growth rate of the cloud droplets for the initial distribution considered by Bott, with an initial mode radius of 10 μm and a total water content of 1 gm^{-3}, just to see if we can replicate the results he obtained.
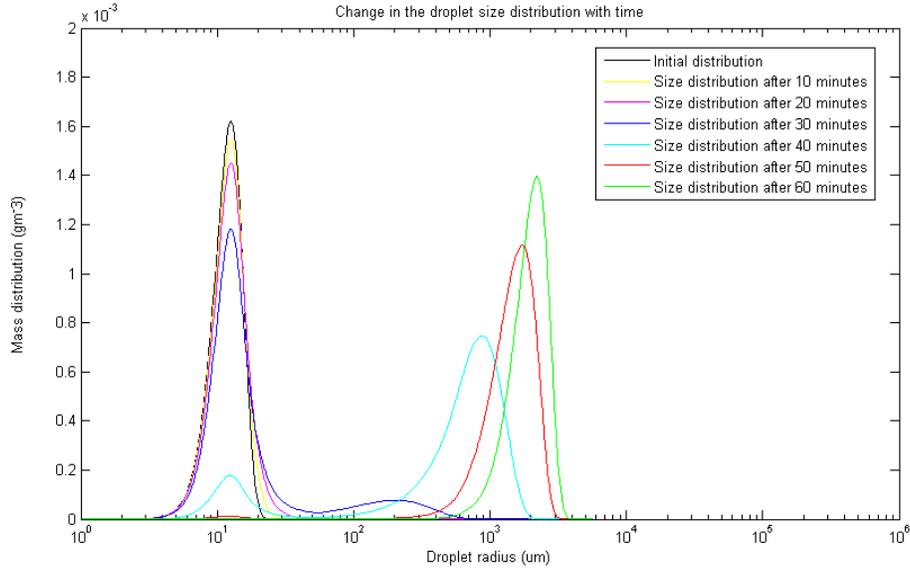
Figure 3.1: Droplet size evolution for an initial mode radius of 10 μm and a total water content of 1 gm^{-3}

From figure 3.1 we can observe that the average size of the droplets clearly increases with time as over the course of an hour the mean radius has become larger by about two orders of magnitude. For the first 30 minutes there does not appear to be a great amount of change in the distribution, with much of the mass still centred in a peak close to 10 μm. The amount of mass in this peak can however be seen to be slowly decreasing in this period, and after 30 minutes there is clear evidence of larger drops having been formed as quite a broad hump, centred close to 200 μm has appeared. The mass in the initial peak is decreasing because drops are colliding and coalescing forming larger drops. If we refer to equation (1.3) we can explain this loss of mass in the initial peak by the first integral, as this represents the increase in the number

of larger drops due to collisions between the smaller (initial) drops.

The most substantial change in the distribution occurs in the 10 minute interval following the distribution described after 30 minutes, as after 40 minutes most of the mass is in a peak centred close to 1 mm (1000 μm), which is quite a shift from the situation seen 10 minutes earlier where most of the mass was still in drops of radius close to 10 μm. An explanation for this sudden shift comes from the fact that we would expect the larger drops that have clearly formed after 30 minutes to rapidly collect the smaller drops. This is thought because if we refer to equation (1.18) it is obvious that the collection kernel will be larger for these type of collisions (compared to that for collisions between the smaller initial drops with other small drops). This is due to the $(r_i + r_j)^2$ component being larger, and also the difference in terminal velocity component $(w(r_i) - w(r_j))$ being larger. Further to this, from equation (1.19) it also clear that the collection efficiency E will be larger since the collector drop r_1 is larger in this collision scenario. So we see this rapid shift in the figure because of the higher collision and coalescence rate for collisions between the larger and smaller drops, compared to that for collisions of small drops with other small drops. For the remaining 20 minutes of the simulation, the peak formed close to 1000 μm can be observed to gain mass and also move to the right in the figure, suggesting the drops are continuing to grow in size. As a result, after 60 minutes the vast majority of the mass is in a peak centred close to 2 mm.

From this we have revealed that the rate of droplet growth is very much

dictated by the collision kernel, which is dependent on the size of the colliding droplets (the kernel value increases with colliding droplet size). We will further investigate this sensitivity to the collision kernel later in the report.
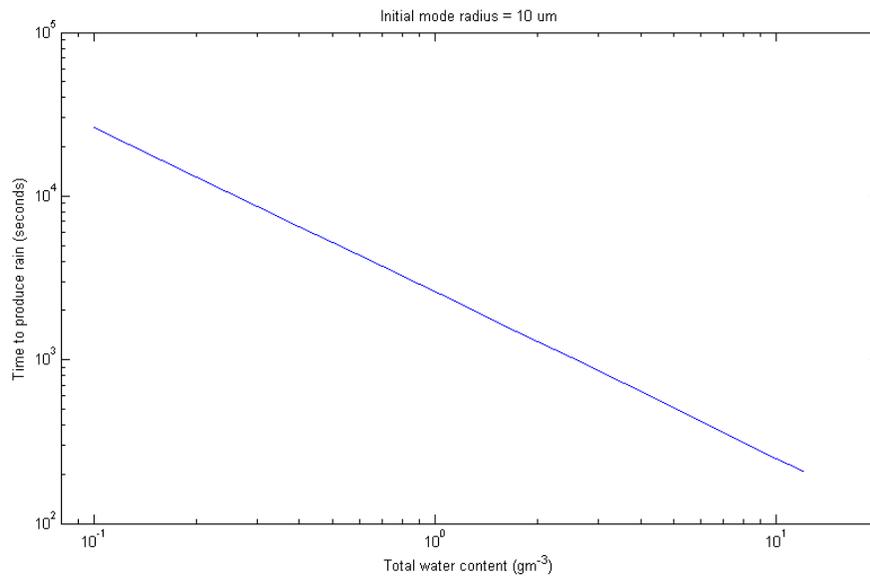

Figure 3.2: Time taken to produce rain for varying total water contents but with the initial mode radius of droplets fixed to 10 μm

We next explore the time taken for the model to produce rain (50% of the mass in drops of radius greater than 1mm), through perturbing the total water content from the default 1 gm^{-3} (figure 3.2). The initial mode radius has not been changed here, so simply increasing the water content gives more drops, and likewise reducing it gives fewer drops. As we might expect, it would appear from the plot that increasing the total water content reduces

the amount of time taken to produce rain. The figure also suggests that there is a minimum water content below which the model does not produce rain, and we can observe that this minimum value is about (0.1 gm^{-3}). It makes sense in practice for such a minimum to exist, because if the total water mass is less than the mass of a 1mm drop, then even if every drop collided and coalesced to eventually form just 1 drop, it would still be too small to be classed as a rain. From the figure it is obvious that in logarithmic axis the gradient of the line is constant, and we find it to be precisely equal to -1. It is therefore clear from the equation for a straight line that we have the relation:

$$log_{10}t \propto -log_{10}w = log_{10}w^{-1},$$

where w is the total water content and t the time taken to produce rain. We can therefore conclude from this that the relation $t \propto w^{-1}$ is valid.
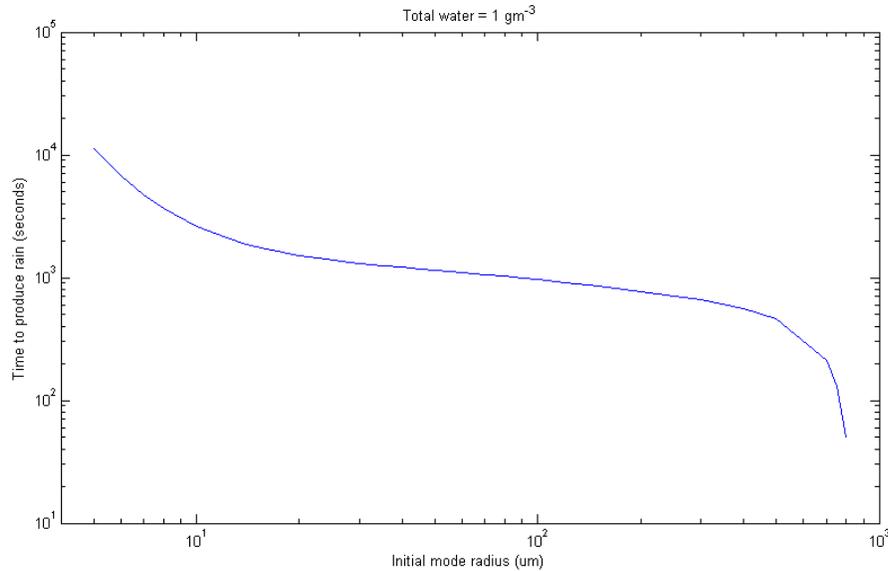
Figure 3.3: Time taken to produce rain for varied initial mode radii but with the total water content fixed at 1 gm^{-3}

We now again investigate the time taken for the model to produce rain, but this time through modifying the initial mode radius as shown in figure 3.3. The total water content is kept constant at 1 gm^{-3} in this analysis, so through increasing the initial mode radius we get fewer, but larger drops. Clearly if we decrease this initial radius we will get smaller drops, but of a greater concentration.

First of all from figure 3.3 we can see that for an initial mode radius of 10μm the time taken to produce rain is close to 40 minutes, which is consistent with figure 3.1. If this initial radius is increased the time taken to produce rain can be observed to reduce, and likewise reducing the initial radii

results in an increasingly longer time taken to achieve rain. It seems from the figure that if the mode radius too small, rain is never produced, which we would expect from the previous work in this field. Figure 3.3 suggests that the initial mode radius must be greater than about 5μm for the collision and coalescence mechanism to produce rain. Through examining the starting distributions for initial mode radii of 4 and 5 μm (figure 3.4), we can observe that for the larger of the two sizes, there are substantially more drops close to and above 10 μm. The fact that an initial mode radius of 5 μm produces rain, but one of 4 μm does not, is actually very much in line with the findings of Davis and Sartor, as they suggested that the collector drops must be larger than 10 μm for growth to occur by collision and coalescence.
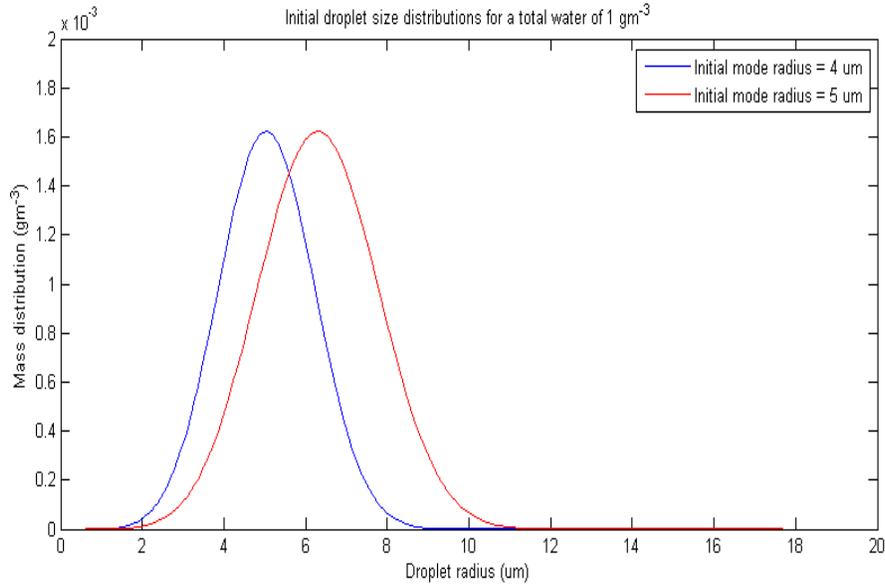
Figure 3.4: Initial droplet size distributions for mode radii of 4 and 5 μm

Figure 3.3 indicates that the relationship is more complex compared to that between the time to produce rain and the total water content. The first aspect to note is that there appears a region on the graph between initial mode radii of 20 and 300 μm where the gradient is almost constant. The gradient in this region is about -1.1, and so the relation $t \propto r^{-1.1}$ approximately holds between the radii specified. To the left of this region, the gradient gradually becomes steeper as the radius decreases, until the minimum initial mode radius required to produce rain is reached. To the right of the straight region, a comparatively rapid steepening of the gradient occurs. It is this region we now investigate to find a best fit to the curve.

From a theoretical perspective if we have initial cloud drops of uniform mass,

then

$$m = \frac{w}{n} \tag{3.1}$$

where w is again the total water content and n is the droplet number concentration. Although we know from equation (1.18) that the collision kernel (droplet interaction rate) increases with droplet size (mass), for simplicity here we consider it to be a constant (λ). For constant λ we have the relation,

$$\frac{dn}{dt} = -\lambda n^2 \tag{3.2}$$

which has the obvious solution,

$$n = \frac{n_0}{1 + \lambda n_0 t} \tag{3.3}$$

where n_0 is the initial droplet number concentration, and n is the number concentration at time t. The droplet mass then evolves like,

$$m = \frac{w}{n} = m_0(1 + \lambda n_0 t). \tag{3.4}$$

where m_0 is the initial mass of the cloud drops, and m is the mass at time t. The time taken to produce rain drops t_r can also be easily determined as:

$$\lambda n_0 t_r = \frac{m_r}{m_0} - 1 \tag{3.5}$$

27

where m_r is the mass of raindrops. Since we have been considering the growth of the cloud droplets in terms of radius increase, as opposed to mass increase, we can use the relation described earlier that $m \propto r^3$ to write,

$$\lambda n_0 t_r = \frac{r_r^3}{r_0^3} - 1 \tag{3.6}$$

where r_r is the radius of raindrops and r_0 is the initial droplet radius. From this analysis we would therefore expect cubic behaviour between t and r.

Traditionally cloud droplets are thought to grow as the square root of time if we just consider the diffusion of moisture onto them, this being due to the relation:

$$\frac{r_1^2 - r_0^2}{2} = v(t_1 - t_0) \tag{3.7}$$

where r_1 and r_0 are the droplet radii at times t_0 and t_1 respectively. Here v effectively represents the rate of diffusion onto the droplets. Although this growth rate does not explain the rapid formation of rain seen in convective clouds, we can use the idea that $t \propto r^2$, or even more broadly that $t \propto r^a$ (where a may be perturbed) as a starting point to investigate the region of rapidly steepening gradient. We therefore consider the following:

$$t = \frac{(r_1^a - r_0^a)}{av} \tag{3.8}$$

Here v we may perturb to achieve the best fit, r_1 in the context of the problem we are considering corresponds to the critical radius at which the time taken to produce rain (t) becomes zero (which we can approximately read off figure 3.3 as 0.08 cm), r_0 represents the initial mode radius of the drops, and a we can perturb to make the relationship between t and r either linear, quadratic, cubic or higher order. It should be noted that r_1 may also be perturbed slightly to improve the fit of the curve to the actual solution.

Equation (3.6) suggested that cubic behaviour should give the best fit to the actual data, however this result was derived at constant collision kernel, which we know not be the case in the model, and so we will investigate a range of values for a.
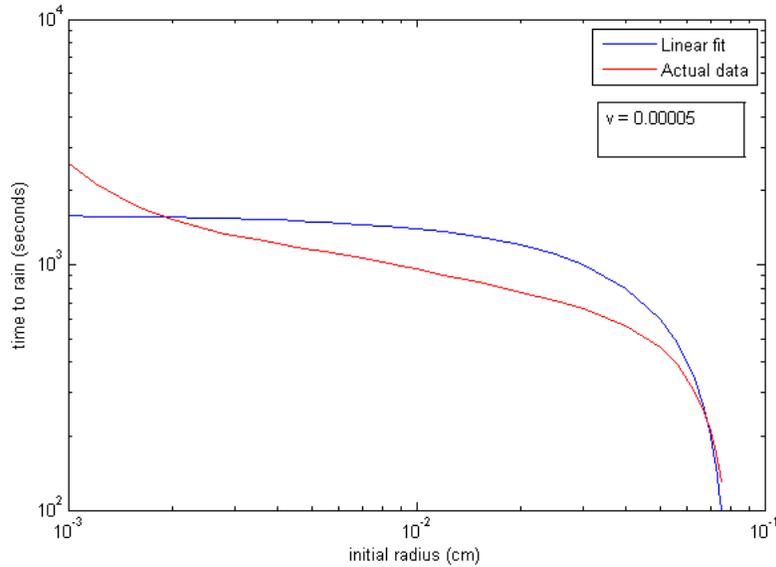
Figure 3.5: Comparing the time taken to produce rain from a fitting curve with a=1, v = 0.00005 and $r_1 = 0.0800$cm to the actual data

If we first try a linear fit ($a = 1$), we can achieve a solution (figure 3.5) that is somewhat comparable to the actual data with $v = 0.00005$ and $r_1 = 0.0800$ cm. The fitting curve generally however has too steeper gradient in the region of interest, as the values of the time taken to produce rain go from being overestimates (in the region between $r_0 = 0.002$ and 0.07 cm) to being underestimates for $r_0 > 0.07$ cm. From this analysis it would appear that the relationship between t and r is not linear, so we now try greater values of a.
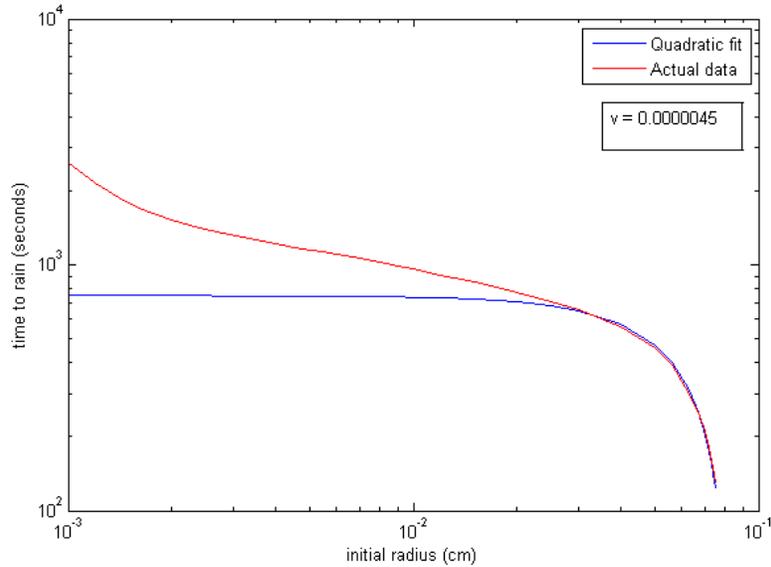
Figure 3.6: Comparing the time taken to produce rain from a fitting curve with a=2, v = 0.0000045 and r_1 = 0.0821cm to the actual data

Figure 3.6 illustrates that a quadratic relation ($a = 2$) with $v = 0.0000045$ and $r_1 = 0.0821$ cm gives a very good representation of the actual data in the region we are concentrating on. The rate of negative increase of the gradient is simulated much better than it was with the linear fit, and also the time to rain values match much better to those of the actual data. If we examine the figure close enough it can be seen however that the rate of change of the gradient is still slightly overestimated, and so we now investigate the solution for $a = 3$.
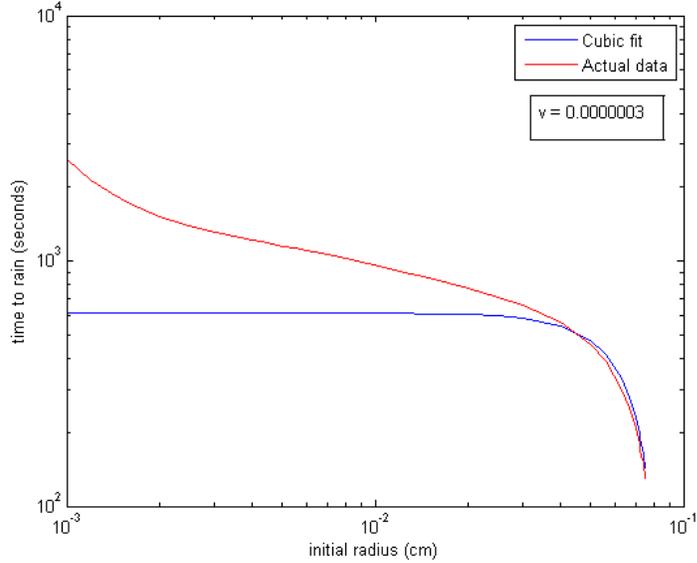
Figure 3.7: Comparing the time taken to produce rain from a fitting curve with a=3, v = 0.0000003 and $r_1 = 0.0820$cm to the actual data

From figure 3.7 we can observe that for $v = 0.0000003$ and $r_1 = 0.0820$ cm (which gives the best fit for this value of a), the solution is more accurate than the linear one, but less so compared to the quadratic. This analysis is therefore not consistent with equation (3.6) which suggested cubic behaviour should give the best fit. The solution is however not substantially less accurate compared to that for $a = 2$, particularly in the region of $r_0 > 0.04$ cm. It is clear that the change in gradient appears once again to be somewhat too rapid close to r_1.

The results we have examined suggest that as we increase the value of a, the radius at which the gradient of the solution begins to change is becoming

larger, and certainly it would seem from figure 3.7 that the change in gradient starts at too large a radius. We therefore will not consider larger values of a.
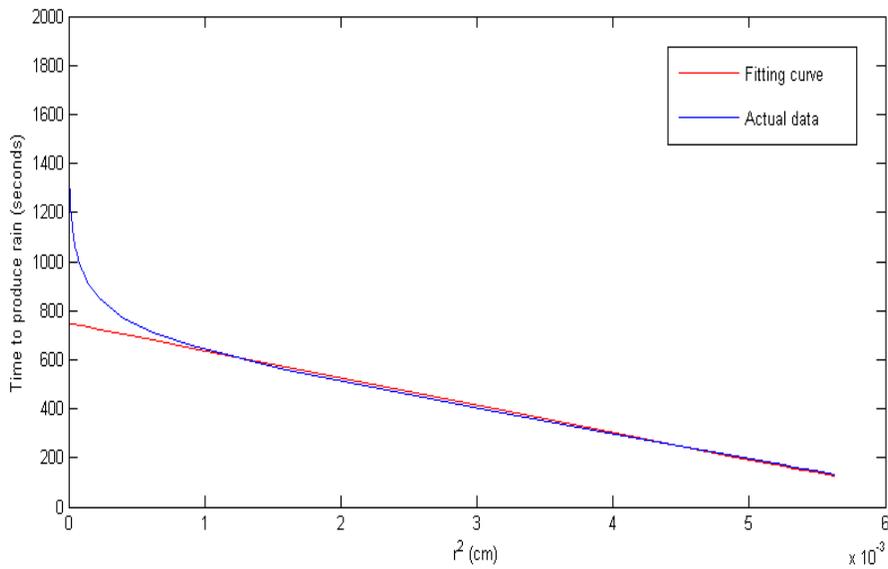

Figure 3.8: Variation of the time taken to produce rain with the square of the initial radius for a=2 as in figure 3.6

We can shown the quality of fit more accurately for the quadratic relation $(a = 2)$ as illustrated in figure 3.8 by plotting the time to rain against the square of the initial mode radius. From this it is clear that the fit is not quite perfect as the gradient of the fitting curve is slightly steeper than the curve corresponding to the actual data, which is what we were able to determine from figure 3.6. However the differences are very minor and to good

33

approximation we can say that in the region of rapidly steepening gradient in figure 3.3, $t \propto r^2$. So this analysis is not consistent with equation (3.6), and the most plausible reason for this is the fact that the collision kernel is taken to be constant in the theory, but in the model it increases with droplet radius.

We next investigate the nature of the droplet growth when there are two peaks in the initial droplet size distribution. We do this so as to examine how the droplets in the two peaks interact, from which we should be able to determine the relative importance (for the formation of rain) of collisions between drops in different peaks and drops in the same peak.
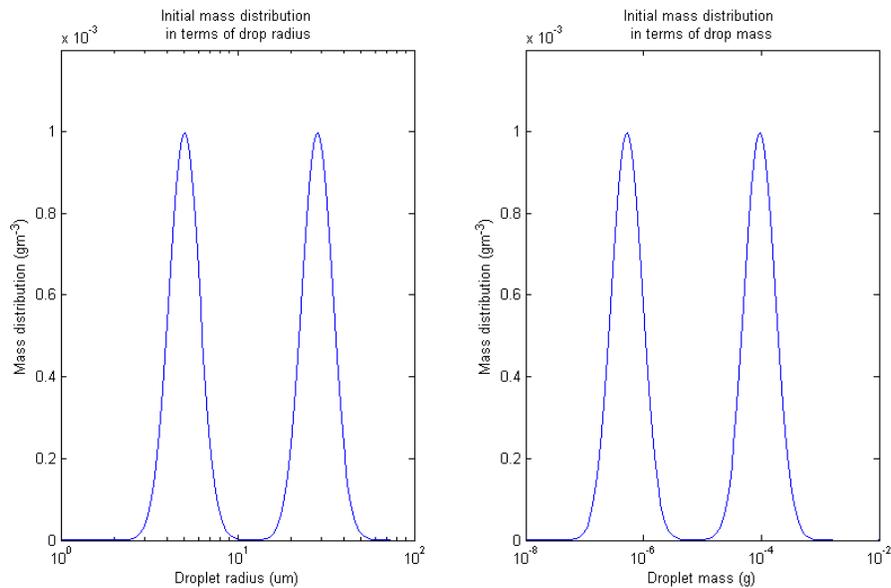

Figure 3.9: Initial distribution with two peaks, shown in terms of droplet mass and radius

We consider the initial distribution shown in figure 3.9 where both peaks are gaussian and identical. The peaks are centred at radii of approximately $5\mu m$ and 30 μm respectively. The mass of the drops in the peaks is also shown in the right hand plot, as the results that follow will consider the evolution of the droplet masses rather than radii.

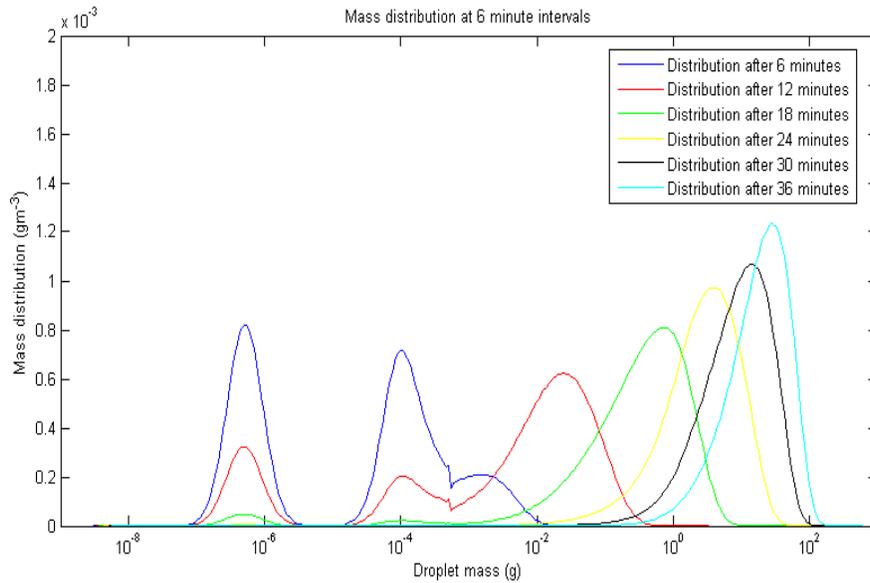Figure 3.10: Droplet mass evolution from the intial distribution shown in figure 3.9

If we first just examine the evolution of the droplet masses with time for the initial distribution with two peaks shown in figure 3.9, we observe that after 6 minutes (figure 3.10), both the initial peaks have lost mass (but are still evident), and a third peak has formed centred close to 2×10^{-3} g. This

third peak can be seen to gain mass at the expense of the initial two for the remainder of the evolution, and also it can be seen to move to the right in the figure (indicating that larger drops are being formed with time).

Theoretically we would expect the droplet number concentrations in the smaller radii peak (n_1) and larger radii peak (n_2) to decrease at the following rates:

$$\frac{dn_1}{dt} = -\lambda n_1 n_2 \tag{3.9}$$

$$\frac{dn_2}{dt} = -\lambda n_1 n_2 \tag{3.10}$$

forming new drops of mass $m_3 = m_1 + m_2$ at a rate

$$\frac{dn_3}{dt} = \lambda n_1 n_2. \tag{3.11}$$

In 3.9 and 3.10 λ represents the interaction rate of the droplets (the collision kernel), which as in the previous theoretical derivation is taken to be constant. In this theoretical example we are just considering drops of mass m_1 and m_2, meaning that the initial distribution is in the form of two spikes at these droplet masses rather than a gaussian curve. Also collisions are not considered to occur between drops of the same mass, which is in fact a true statement if we refer back to equation (1.18) since $w(r_i) - w(r_j)$ will be zero. Since m_1 is small, m_2 and m_3 are close together, and so we can replace the two spikes at m_2 and m_3 with a single spike of mass:

$$m_l = \frac{n_2 m_2 + n_3 m_3}{n_2 + n_3} \tag{3.12}$$

and drop number concentration,

$$n_l = n_2 + n_3. \tag{3.13}$$

Since n_3 will increase at the expense of n_2, we see that m_l increases at the following rate:

$$m_l = m_2 + \frac{n_3}{n_2 + n_3} m_1, \tag{3.14}$$

so that,

$$\frac{dm_l}{dt} = \frac{dn_3/dt}{n_2 + n_3} m_1 = \frac{\lambda n_1 n_2}{n_2 + n_3} m_1. \tag{3.15}$$

After the first timestep (for which $n_3 = 0$) we associate the new peak at m_l with m_2 (and n_l with n_2) and set $n_3 = 0$ again. We therefore find that:

$$\frac{dn_1}{dt} = -\lambda n_1 n_2 \tag{3.16}$$

$$\frac{dn_2}{dt} = 0 \tag{3.17}$$

$$\frac{dm_l}{dt} = \lambda n_1 m_1 \tag{3.18}$$

We would expect this simplification of the initial distribution (from gaussian

curves to single spikes) in figure 3.9 to give a mass evolution that has reasonable similarity to that shown in figure 3.10. It is however immediately obvious that the third peak that forms in figure 3.10 has a mass at all time intervals that is substantially larger than $m_1 + m_2$, and so it would appear that critical detail is missing from the theoretical calculations.

We can examine using the collision efficiency calculated according to Hall, rather than that by Long, to see if this results in any substantial differences in the evolution of the droplet masses.
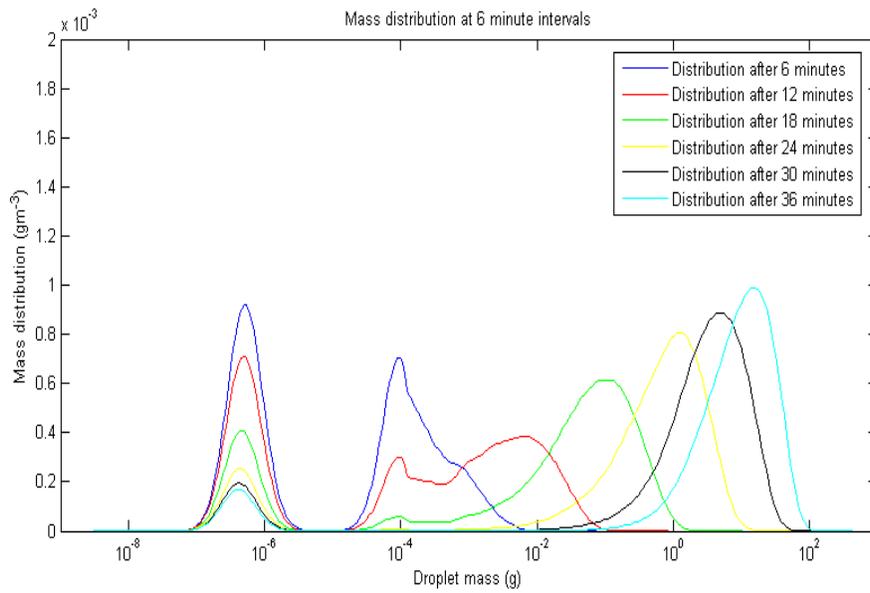

Figure 3.11: Droplet mass evolution from the intial distribution shown in figure 3.9 but with the collision efficiency calculated according to Hall

It is apparent from figure 3.11 that the formation of the larger drops is slightly slower when this different collision efficiency is considered (compared to figure 3.10), however the results still disagree with the evolution we would expect from the theoretical approach. To try to explain this we must remember that we have not considered a gaussian distribution in the theory, and so we are missing some larger (and indeed smaller) drops compared to the distribution in figure 3.9. Also the collision kernel is taken to be constant which we know not to be the case from equation (1.18). It seems unlikely that the extra smaller drops are of critical importance (since no combination of them can really produce the mass evolutions shown in figures 3.10 and 3.11). It is however possible that the few very largest drops in the larger radii gaussian peak that are not considered by the theoretical calculations could be of critical importance in explaining the evolutions that the figures show.

So we are proposing that it is the very largest drops that dominate the growth process and that they are necessary for rain to be formed. The problem is however that the number concentration of drops of this size is comparatively very low to those of smaller size, and so it seems that for these drops to be important, they must have a substantially higher chance of colliding and coalescing with each other compared to the smaller drops. As previously stated, we know from equation (1.18) that this chance does increase with colliding droplet size, but it seems that this increase is actually very rapid indeed from figures 3.10 and 3.11. We can explore this by calculating the magnitude of the kernel for different size drop collisions. We can even com-

pute the components that contribute to the kernel, to try to find the main reason or reasons for the changes in value.

Different collision scenarios	Kernel calculated using Long (1974) collision efficiency	Kernel calculated using Hall (1980) collision efficiency
Scenario 1: Collisions between drops not in same peak (considering radii of 5um and 30um)	Value	Value
Contribution from terminal velocity (ms^{-1})	1.00E+01	1.00E+01
Contribution from radius (m^2)	1.24E-05	1.24E-05
Contribution from collision efficiency	1.66E-01	3.94E-02
Kernel	6.47E-05	1.54E-05
Scenario 2: Collisions between 30um and 60um drops	Value	Value
Contribution from terminal velocity (ms^{-1})	2.34E+01	2.34E+01
Contribution from radius (m^2)	8.20E-05	8.20E-05
Contribution from collision efficiency	1.00E+00	9.11E-01
Kernel	6.01E-03	5.48E-03
Scenario 3: Collisions between 5um and 10um drops	Value	Value
Contribution from terminal velocity (ms^{-1})	9.13E-01	9.13E-01
Contribution from radius (m^2)	2.28E-06	2.28E-06
Contribution from collision efficiency	1.85E-02	3.31E-02
Kernel	1.21E-07	2.16E-07
Scenario 4: Collisions between 30um and 13um drops	Value	Value
Contribution from terminal velocity (ms^{-1})	8.26E+00	8.26E+00
Contribution from radius (m^2)	1.87E-05	1.87E-05
Contribution from collision efficiency	3.16E-01	4.72E-01
Kernel	1.53E-04	2.29E-04
Scenario 5: Collisions between 5um and 2.5um drops	Value	Value
Contribution from terminal velocity (ms^{-1})	2.30E-01	2.30E-01
Contribution from radius (m^2)	5.71E-07	5.71E-07
Contribution from collision efficiency	3.79E-05	4.00E-02
Kernel	1.57E-11	1.65E-08

Figure 3.12: Table showing the components of the Kernel with the collision efficiency calculated according to Long (1974) and Hall (1980)

In figure 3.12 we have compared the components that make up the kernel, and the kernel itself for different possible colliding scenarios for the initial

40

two peak distribution we have been considering. If we first just consider the value of the kernel when the collision efficiency from Long is used, we can see that for collisions between drops not in the same peak it has value of order 10^{-5}. This value is a factor of 100 smaller than the kernel for collisions between the very largest drops in the initial distribution (radii of 60 μm) and averaged sized drops in the larger radii peak (30 μm radius). Also if we consider collisions between averaged sized drops in the smaller radii peak (5 μm radius) with the very smallest drops in this same peak (2.5 μm radius) the kernel has value of order 10^{-11}, which suggests that very few, if any drops of this size collide and coalesce (which we would expect from Davis and Sartor 1967). These results tell us that the kernel is indeed very sensitive to the radii of the colliding drops, as its value increases very rapidly as the colliding drop radii increase.

If we now examine the individual components of the kernel, we should be able to determine the main contributing factor (or factors) that lead to the great sensitivity to the drop radii. Looking first at the difference in terminal velocity component, we can see that this varies between 2×10^{1} and 2×10^{-1} for the most extreme comparison (between scenario 2 and 5), corresponding to a factor difference of 100. The component from the colliding drop radii ($(r_i+r_j)^2$) for these two scenarios has value 8×10^{-5} and 6×10^{-7} respectively, and so this component differs by a factor of about 135. For these same two scenarios, the contribution from the collision efficiency (from Long 1974) is 1 and 4×10^{-5} respectively and so this component has the largest factor difference of 2.5×10^{4}. It therefore seems that certainly when Long's efficiency is

used, the dominant component that causes the rapid change in kernel value with drop size is the collision efficiency. It should be noted however that all the components make a positive contribution to the change in kernel value with increasing colliding drop radii.

We now turn our attention to the collision efficiency determined according to Hall. Since the colliding droplet radii and terminal velocity difference contributions are the same, we will simply examine the collision efficiency values for the different scenarios. First if we look at the collision of the smallest drops (scenario 5), we have a collision efficiency of 4.0×10^{-2}, which is over 1000 times larger than for the same scenario with the collision efficiency calculated according to Long. This highlights that the collisions of these small drops are much more likely (important) when the collision efficiency is determined as in Hall. For collisions between the biggest drops (scenario 2), the collision efficiencies are much more comparable, although this time the Long efficiency is the larger, however this is only by about 10 %. Considering collisions between drops not in the same peak (scenario 1), we find that the Hall efficiency is actually slightly smaller compared to in scenario 5. This is in great contrast to the Long efficiency which is about 3 times larger than the Hall efficiency in scenario 1, but obviously the difference between the Long efficiencies for scenarios 1 and 5 is very large. From this analysis it appears that whilst both efficiencies show the few larger drops to be of the most importance, they disagree substantially on the likelihood of collisions between very small drops and also to a lesser extent on collisions of drops that are not in the same peak.

We can relate these findings to figures 3.10 and 3.11 to see if we can now better explain the differences in the evolution of the droplet masses. Firstly figure 3.12 showed that the Long efficiency is about 3 times greater than that of Hall for collisions between drops, not in the same peak. We would therefore expect the smaller radii peak to lose mass quicker with the kernel calculated using the Long efficiency, and it is clear that this is the case through simply comparing the figures. The fact that Hall's efficiency is slightly lower than Long's for collisions between the largest drops means we may expect the formation of larger drops to be slowed in figure 3.11 compared to figure 3.10 which is indeed what we do observe. The substantially higher Hall efficiency for collisions between drops in the smaller radii peak appears to have little effect from the figures, but we should expect this because the overall kernel value for collisions of drops this small is still very low. It can therefore be said that the findings in figure 3.12 do agree with the droplet mass evolutions obtained.

As a final investigation we now fix the kernel to examine as to whether or not we observe the kind of growth pattern shown in figures 3.10 and 3.11. The results in figure 3.12 suggest we should not expect the rapid formation of very large drops if we fix the kernel to a value much lower than it would be if we allowed it to vary.
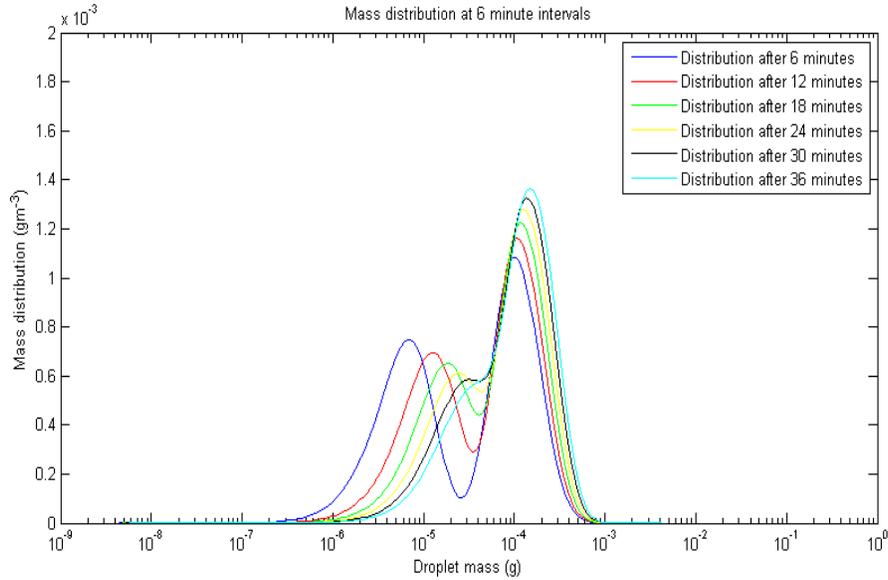
Figure 3.13: Evolution of the droplet masses for a fixed collision kernel of 0.00001

The effect of fixing the kernel to 0.00001 is clearly quite profound (figure 3.13) as large drops of rain size do not form, and the larger peak that does form has mass that is simply the progressive sum of the smaller and larger initial drops. From this evidence it is clear that the rapid increase in the kernel with droplet size is of great importance for the formation of rain, as is the presence of a few larger drops (that we have from a gaussian distribution).

Chapter 4

Conclusion

In conclusion we have been able to obtain useful results for the perturbations considered to the initial cloud droplet distribution. Through examining the droplet size evolution with time for the initial conditions considered by Bott, we were able to show that once a few larger droplets have formed, the small initial drops are very rapidly collected by these large drops, and all the water mass in the cloud quickly shifts to be just in large droplets. This could be explained by the theory and equations in the model, which showed that larger drops collide and coalesce with other drops more readily than smaller drops.

We then investigated changing the total water content within the cloud, and were able to show that if we increase the amount of water, the model produces drops of rain size more quickly. It was hence possible to confirm that the relationship $t \propto w^{-1}$ is valid for all water contents. The relationship between the initial mode radius of the cloud drops and the time taken to

produce rain was more complex, although it was obvious that if the initial radius was increased for a fixed total water content, drops of rain size were produced more rapidly. For an initial mode radius $20\mu m \leq r \leq 300\mu m$ the relationship $t \propto r^{-1.1}$ approximately holds. For $r > 300\mu m$ we investigated a relationship of the form

$$t = \frac{(r_1^a - r_0^a)}{av}$$

and tried to achieve the best fit to the actual data with $a = 1, 2, 3$ corresponding to a linear, quadratic and cubic relationship. The best match was achieved with $a = 2$ (a quadratic fit), $v = 0.0000045$ and $r_1 = 0.0821$ cm. Therefore for $r > 300\mu m$ it seemed that to good approximation $t \propto r^2$. This result disagreed with the cubic behaviour that was expected from a theoretical result derived at constant kernel, with the best explanation for this being that the variation of the kernel with colliding drop radii is very important and cannot be neglected (which we later showed to be the case).

It appeared that to produce rain drops the initial mode radius had to be at least $5\mu m$, and through analysing the initial droplet size distribution that this corresponds to we were able to support the claims of Davis and Sartor that collector drop radii must be at least $10\mu m$ for droplets to grow by collision and coalescence. The conclusion here is that drops of radius less than 10 μm will not collide and coalesce with similar size drops. The reason for this is that drops of this size have little difference in terminal velocity. The combination of this and the fact that such drops have little inertia to motion,

means they will follow the air flow around each other rather than colliding.

Through considering an initial droplet distribution with two peaks we were able to show that the model shifts much of the initial mass into substantially larger drops very quickly. This rate of larger drop formation could not be explained by simple theoretical calculations derived at constant kernel, which considered collisions between drops of size equal to the mean size in each peak. This was also true when the collision kernel was adapted in the model to include the collision efficiency from Hall as opposed to that from Long. It seemed likely therefore that not accounting for the few larger drops with higher collision kernel in this initial distribution, was causing the theoretical calculations to disagree. However since the number concentration of such drops was so low, it appeared likely that the chance of these drops colliding and coalescing was not just gradually increasing with colliding drop radii, but actually rapidly increasing.

Through investigating the values of the collision kernel we were able to show that regardless of which method (Long or Hall) was used to obtain the collision efficiency, a very large difference (10^8 for Long and 10^5 for Hall) existed between the kernel values for the two most extreme collision scenarios in the initial distribution. By most extreme we mean at the one extreme, collisions of the very largest drops present with other large drops (giving the highest kernel values), and at the other extreme, collisions of the very smallest drops with other small drops (giving the lowest kernel values). This showed that the chance of the larger drops colliding and coalescing is indeed substantially

higher, compared to the chance for smaller drops.

It was shown that out of the three components that make up the kernel, the dominant one that causes much of the increase in kernel value with colliding drop radii was the collision efficiency, when it was calculated according to Long. This was not however the case when the collision efficiency was determined according to Hall, as the three components were comparable in size and so equally responsible for the kernel increase. The effect of the different collision efficiencies could be seen to cause slightly different droplet mass evolutions. When the Long efficiency was used the drops in the smaller radii peak collided and coalesced with drops from the other peak faster compared to when the Hall efficiency was used. Also the formation of a third peak (larger drops) was slightly delayed when the Hall efficiency was used instead of that of Long.

Finally through fixing the kernel to a value close to what we would expect for collisions of drops of average size in the initial distribution, it was illustrated that fast production of large (rain) drops does not occur (at least not in the time periods we were considering). This proved that the few large drops in the initial distribution (which collide and coalesce readily due to there large kernel values) are essential for the fast production of rain in convective clouds.

It would seem from the results we have obtained, that we can replicate the rapid droplet growth rates that must occur in convective clouds to produce rain in such short time periods. It is however the case that we have obtained

seemingly realistic growth rates from cloud droplet distributions that may or may not be realistic. For this reason it would be ideal to test this model on a known real distribution in a cloud (although it would be difficult to ever measure this accurately). If this were possible, we could then be confident that we are simulating the growth process correctly (provided the model produces rain in a time comparable to reality).

A future aspect that could be incorporated into the model is turbulence, especially when convective clouds have substantial updraughts and down-draughts. These are likely to lead to collisions between drops, and as a result the time taken to produce rain may be quicker. On the other hand accounting for turbulence may prevent collisions occurring between certain drops, due to its effects lessening the importance of terminal velocity differences.

Chapter 5

References

Hocking, L. M., 1959: The collision efficiency of small drops. *Quart. J. Roy. Meteor. Soc.,* **85**, 44-50.

Davis, M. H., and J.D. Sartor, 1967: Theoretical collision efficiencies for small cloud droplets in Stokes flow. *Nature.,* **215**, 1371-1372.

Davis, M. H., 1972: Collisions of small droplets: Gas kinetic effects. *J. Atmos. Sci.,* **29**, 911-915.

Jonas, P. R., 1972: The collision efficiency of of small drops. *Quart. J. Roy. Meteor. Soc.,* **98**, 681-683.

Schlamp, R. J., S. N. Grover, H. R. Pruppacher and A. E. Hamielec, 1976: A numerical investigation of the effect of electric charges and vertical external fields on the collision efficiency of cloud drops. *J. Atmos. Sci.,* **33**, 1747-1755.

Lin, C. L., and S. C. Lee, 1975: Collision efficiency of water drops in the atmosphere. *J. Atmos. Sci.,* **32**, 1412-1418.

Shafrir, U., and T. Gal-Chen, 1971: A numerical study of collision efficiencies

and coalescence parameters for droplet pairs with radii up to 300 microns. *J. Atmos. Sci.,* **28**, 741-751.

Klett, J. D., and M. H. Davis, 1973: Theoretical collision efficiencies of cloud droplets at small Reynods numbers. *J. Atmos. Sci.,* **30**, 107-117.

Beard, K. V., and H.T. Ochs, 1984: Collection and coalescence efficiencies for accretion. *J. Geophs. Res.,* **89**, 7165-7169.

Pruppacher, H. R., and J. D. Klett, 1997: *Microphysics of Clouds and Precipitation.* Kluwer Academic, 954 pp.

Berry, E. X., and R. L. Reinhardt, 1974: An analysis of cloud droplet growth by collection: Part 1. Double distributions. *J. Atmos. Sci.,* **31**, 1814-1824.

Bott, A., 1998: A Flux Method for the Numerical Solution of the Stochastic Collection Equation. *J. Atmos. Sci.,* **55**, 2284-2293.

——, 1989a: A positive definite advection scheme obtained by nonlinear renormalization of the advective fluxes. *Mon. Wea. Rev.,* **117**, 1006-1015.

——, 1989b: Reply. *Mon. Wea. Rev.,* **117**, 2633-2636.

Kovetz, A., and B. Olund, 1969: The effect of coalescence and condensation on rain formation in a cloud of finite vertical extent. *J. Atmos. Sci.,* **26**, 1060-1065.

Golovin, A. M., 1963: The solution of the coagulation equation for cloud droplets in a rising air current. *Izv. Akad. Nauk. SSSR. Ser. Geofiz.,* **5**, 783-791.

Beard, K. V., 1976: Terminal velocity and shape of cloud and precipitation drops aloft. *J. Atmos. Sci.,* **33**, 851-864.

Long, A., 1974: Solutions to the droplet collection equation for polynomial kernels. *J. Atmos. Sci.,* **31**, 1040-1052.

Hall, W. D., 1980: A detailed microphysical model within two-dimensional dynamic framework: Model description and preliminary results. *J. Atmos. Sci.,* **37**, 2486-2507.